An Introduction of Boundary Element Method to the Analysis of Crack Propagation in Concrete

Abd. Latif Saleh
Department of Structures and Materials
Faculty of Civil Engineering

Abstract

The dual boundary element method (DBEM) incorporated with fictitious crack model (FCM) is used to analyse and simulate the crack propagation in concrete. The fracture in concrete is represented by the FCM in which the fracture zone is replaced by applying closing forces on both crack surfaces. When the force at the fictitious crack tip exceeds the maximum tensile strength of the concrete, the fictitious crack will propagate perpendicular to the maximum principal stress. Three–point bending specimen is used to check the numerical analysis and the results is compared to the analysis by finite element method and experimental results.

1 Introduction

The boundary element method (BEM) is nowadays recognized as an efficient numerical technique appropriate to solve many engineering problems [1]. The method appears to be particularly recommended to solve crack problems mainly due to the simple discretization and remeshing required by the technique. Several fracture mechanics formulations in the standard BEM have already been developed. These formulations has been presented and discussed in many publications, such as Aliabadi & Rooke [2] and also in Cruse [3]. In

this paper an alternative formulation to deal with crack analysis in concrete is proposed. The procedure is derived from the well known dual boundary element method (DBEM) and the fictitious crack model (FCM).

The DBEM reported by Portela, Aliabadi & Rooke [4] has been established as an alternative to solve the general mixed mode crack propagation using a single–region formulation. The technique is based on the displacement boundary integral equation applied on one of the crack surfaces and traction boundary integral equation on the other crack surface. This method overcomes the difficulty of modelling the crack surfaces in the conventional BEM as two coincident source points are in the same integration path. The DBEM allows the simulation of crack growth in a straight forward manner without remeshing as the crack path is calculated from the previous step. The application of boundary element method (BEM) to the analysis of cracking in concrete is relatively new and there are only a few publications on the subject. Cen & Maier [5] for example, used the multidomain BEM to simulate crack propagation in concrete. Later Saleh & Aliabadi [6] extended the DBEM formulation to include cohesive forces to represent the fracture zone in concrete.

On the other hand, FCM is used to simulate fracture zone occuring in concrete when it is subjected to tensile loading. The FCM is a theory applicable to numerical calculation of crack propagation in concrete structure or a structure of similar materials having a low ultimate tensile stress [7]. The application of FCM using the finite element method (FEM) is well established either for mode I or mixed mode crack propagation which has been reported, for example by Petersson [8], Ingraffea & Gerstle [9], Carpinteri and Valente [10] and Gerstle & Xie [11].

In this paper, the three–point bending test specimen is used to demonstrate the results using the BEM approach. The results are compared with the results by FEM analysis and experimental results.

2 The fictitious crack model

The FCM is based on the assumption that the fracture zone starts to develop at one point when the maximum principal stress reaches the maximum tensile stress of the material. The fracture zone

develops perpendicular to the maximum principal stress. The material in the fracture zone is partly destroyed but is still able to transfer stress. The stress is dependent on the crack opening displacement. It is also assumed that the material properties outside the fracture zone are linear elastic and given by the $\sigma - \epsilon$ relationship. In the numerical implementation, the fracture zone is replaced by the closing force (or cohesive force) acting on both crack surfaces in which the intensity of these forces is dependent on the crack opening displacement. This crack that appears on the particular viewing surface of the concrete is not a real crack but rather a fictitious crack. Fig. 1(a) shows these forces acting on both sides of the crack in the fracture zone. The linear and bilinear variation of stress–displacement is considered as shown in Fig. 1(b) and 1(c).

The iteration process of the crack propagation is controlled by the crack length as a monotonic increasing function. At every iteration, the final deformation of the structure can be evaluated. Hence, the crack opening displacement can be calculated as a post–processing parameter, once the final deformation was performed. When the crack opening displacement is greater than the critical value, Δu_c, the fictitious will become a real crack (traction–free crack). The elastic–softening fracturing process for the linear stress–deformation curve (SL) can be summarized as follows:

$$\begin{array}{lcll} \sigma & = & E_c\epsilon & \text{for} \quad \epsilon \leq \epsilon_u \\ \sigma_{(\Delta u^{cr})} & = & f'_t\left(1 - \frac{\Delta u^{cr}}{\Delta u_c}\right) & \text{for} \quad 0 \leq \Delta u^{cr} \leq \Delta u_c \\ \sigma_{(\Delta u^{cr})} & = & 0 & \text{for} \quad \Delta u^{cr} > \Delta u_c \end{array} \qquad (1)$$

where σ, ϵ and E_c are the stresses, the strains and Young's modulus of concrete, respectively; f'_t and ϵ_u are the ultimate tensile strength and the ultimate tensile strain of concrete respectively; and $\sigma_{(\Delta u^{cr})}$ is the stress corresponding to the crack opening, Δu^{cr}, at the fictitious crack.

3 DBEM formulation for the fictitious crack model

The dual equations, on which the DBEM is based, are the displacement boundary integral equation and traction boundary integral equation. The boundary integral representation of the displacement components can be written in terms of the boundary point

as

$$c_{ij}(\mathbf{x}')u_i(\mathbf{x}') + \int_\Gamma T_{ij}(\mathbf{x}',\mathbf{x})u_j(\mathbf{x})\mathrm{d}\Gamma(\mathbf{x}) = \int_\Gamma U_{ij}(\mathbf{x}',\mathbf{x})t_j(\mathbf{x})\mathrm{d}\Gamma(\mathbf{x}) \tag{2}$$

where i and j denote Cartesian components, $T_{ij}(\mathbf{x}',\mathbf{x})$ and $U_{ij}(\mathbf{x}',\mathbf{x})$ represent the Kelvin traction and displacement fundamental solutions, respectively. The coefficient $c_{ij}(\mathbf{x}')$ is given by $\delta_{ij}/2$ for the smooth boundary at the point $\mathbf{x}'$ (δ_{ij} is the Kronecker delta) and $\int$ the Cauchy principal value integral.

The boundary integral representation of the traction components, can be written for a point on a crack surface as

$$c_{ij}(\mathbf{x}')t_j(\mathbf{x}') + n_i(\mathbf{x}')\int_\Gamma S_{kij}(\mathbf{x}',\mathbf{x})u_k(\mathbf{x})\mathrm{d}\Gamma(\mathbf{x}) = n_i(\mathbf{x}')\int_\Gamma D_{kij}(\mathbf{x}',\mathbf{x})t_k(\mathbf{x})\mathrm{d}\Gamma(\mathbf{x}) \tag{3}$$

where $S_{kij}(\mathbf{x}',\mathbf{x})$ and $D_{kij}(\mathbf{x}',\mathbf{x})$ are linear combinations of derivatives of $T_{ij}(\mathbf{x}',\mathbf{x})$ and $U_{ij}(\mathbf{x}',\mathbf{x})$, respectively. The n_i denotes the ith component of the unit outward normal to the boundary at point $\mathbf{x}'$. The coefficient $c_{ij}(\mathbf{x}')$ is given by $\delta_{ij}/2$ for the smooth boundary and $\int$ denotes the Hadamad principal value integral.

In FCM, the cohesive forces in the fracture zone create an extra unknown which should be evaluated simultaneously during each of the iteration processes. These forces are related to tractions by the definition of the DBEM context. They can be introduced into the dual boundary element formulation by separating the boundary into two parts, i.e. the non-crack boundary represented by Γ and the crack boundary represented by Γ_{cr}. Hence, the boundary integral of the displacement components, eqn (2) can be written in terms of boundary point as

$$\begin{aligned} c_{ij}(\mathbf{x}')u_i(\mathbf{x}') &+ \int_{\Gamma-\Gamma_{cr}} T_{ij}(\mathbf{x}',\mathbf{x})u_j(\mathbf{x})\mathrm{d}\Gamma(\mathbf{x}) \\ &+ \int_{\Gamma_{cr}} T_{ij}(\mathbf{x}',\mathbf{x})u_j^{cr}(\mathbf{x})\mathrm{d}\Gamma_{cr}(\mathbf{x}) \\ &- \int_{\Gamma_{cr}} U_{ij}(\mathbf{x}',\mathbf{x})t_j^{cr}(\mathbf{x})\mathrm{d}\Gamma_{cr}(\mathbf{x}) \\ &= \int_{\Gamma-\Gamma_{cr}} U_{ij}(\mathbf{x}',\mathbf{x})t_j(\mathbf{x})\mathrm{d}\Gamma(\mathbf{x}) \end{aligned} \tag{4}$$

where $u_j^{cr}(\mathbf{x})$ is the component of the displacement and $t_j^{cr}(\mathbf{x})$ is the unknown distributed cohesive forces applied at one of the crack surfaces, Γ_{cr}.

The boundary integral representation of the traction components, eqn (3), can be written for a point on a crack surface as

$$\begin{aligned} c_{ij}(\mathbf{x}')t_j(\mathbf{x}') &+ n_i(\mathbf{x}')\int_{\Gamma-\Gamma_{cr}} S_{kij}(\mathbf{x}',\mathbf{x})u_k(\mathbf{x})\mathrm{d}\Gamma(\mathbf{x}) \\ &+ n_i(\mathbf{x}')\int_{\Gamma_{cr}} S_{kij}(\mathbf{x}',\mathbf{x})u_k^{cr}(\mathbf{x})\mathrm{d}\Gamma_{cr}(\mathbf{x}) \\ &- n_i(\mathbf{x}')\int_{\Gamma_{cr}} D_{kij}(\mathbf{x}',\mathbf{x})t_k^{cr}(\mathbf{x})\mathrm{d}\Gamma_{cr}(\mathbf{x}) \\ &= n_i(\mathbf{x}')\int_{\Gamma-\Gamma_{cr}} D_{kij}(\mathbf{x}',\mathbf{x})t_k(\mathbf{x})\mathrm{d}\Gamma(\mathbf{x}) \end{aligned} \tag{5}$$

where $u_j^{cr}(\mathbf{x})$ is the component of the displacement and $t_j^{cr}(\mathbf{x})$ is the unknown distributed cohesive forces applied at the other crack surfaces, Γ_{cr}. For traction–free cracks, $t_j^{cr} = t_k^{cr} = 0$. Equations (4) and (5) constitute the basis of the DBEM to include an extra unknown of the cohesive forces in the formulation.

Equation (4) and (5) can be expressed in matrix form as

$$\begin{bmatrix} A & [H_{cr}] & [G_{cr}] \\ 0 & [C_{cr}] & [D_{cr}] \end{bmatrix} \begin{Bmatrix} X \\ \{u_{cr}\} \\ \{t_{cr}\} \end{Bmatrix} = \begin{Bmatrix} F \\ \{S_{cr}\} \end{Bmatrix} \tag{6}$$

in which A is a coefficient corresponding to the vector X containing the unknowns u and t, and F contains the known values of $\overline{u}$ and $\overline{t}$ for the non–crack boundary. $[H_{cr}]$ and $[G_{cr}]$ are coefficients corresponding to the unknown displacement u_{cr} and the unknown cohesive forces t_{cr} respectively, for the crack boundary. $[C_{cr}]$ and $[D_{cr}]$ are the fictitious crack boundary conditions corresponding to the vector $\{u_{cr}\}$ and $\{t_{cr}\}$ respectively; and vector $\{S_{cr}\}$ is a material parameter. For the linear relation of $\sigma - \Delta u^{cr}$, matrices $[C_{cr}]$ and $[D_{cr}]$ contain 4×4 submatrices given by

$$[C_{cr}] = \begin{bmatrix} -\frac{f_t'}{\Delta u_c} & 0 & \frac{f_t'}{\Delta u_c} & 0 \\ 0 & -1 & 0 & 1 \\ 0 & 0 & 0 & 0 \\ 0 & 0 & 0 & 0 \end{bmatrix}, \quad [D_{cr}] = \begin{bmatrix} 1 & 0 & 0 & 0 \\ 0 & 0 & 0 & 0 \\ 1 & 0 & 1 & 0 \\ 0 & 1 & 0 & 1 \end{bmatrix} \tag{7}$$

and vectors $\{u_{cr}\}$, $\{t_{cr}\}$ and $\{S_{cr}\}$ are given by

$$\{u_{cr}\} = [N] \begin{Bmatrix} u_x^a \\ u_y^a \\ u_x^b \\ u_y^b \end{Bmatrix}, \quad \{t_{cr}\} = [N] \begin{Bmatrix} t_x^a \\ t_y^a \\ t_x^b \\ t_y^b \end{Bmatrix}, \quad \{S_{cr}\} = \begin{Bmatrix} f_t' \\ 0 \\ 0 \\ 0 \end{Bmatrix}, \tag{8}$$

where $[N]$ is the transformation matrix from the global to the local reference system varying node by node on the fictitious crack surface. a denotes one of the crack surface and b for the other.

4 Crack modelling strategy

The general modelling strategy developed in the present paper can be summarized as follows [12]:

i. The crack boundaries are modelled with discontinuous quadratic elements, as shown in Fig. 2.

ii. The displacement boundary integral equation, eq. (4), is applied when the source point is located on one of the crack boundary.

iii. The traction boundary integral equation, eq. (5), is applied when the source point is located on the opposite crack boundary.

iv. The displacement boundary integral equation, eq. (4), is applied when the source point is located on the remaining non–crack boundaries of the body.

v. Continuous quadratic element are used along the remaining boundary of the body, except at the intersection between a crack and an edge, where discontinuous elements are required on the edge in order to avoid a common node at the intersection (see Fig. 2).

The above modelling strategies are the key points of the DBEM. For a given crack problem, once the modelling strategy is defined, the discretization of the boundary was followed and then the final step was to transform the integral equation into a system of linear algebraic equations, from which the unknown discrete boundary variables could be obtained.

5 Numerical examples

A series of numerical simulations were conducted to demonstrate the ability of the developed boundary element program to capture the behaviour of the nonlinear fracture zone in concrete materials. The simulations include the comparison with the finite element method and experimental results.

5.1 Example 1: the development of the fracture zone

Fig. 3 shows a notched beam subjected to three–point bending and the material properties used in the analysis. It is assumed that the $\sigma - \epsilon$ curve and the $\sigma - \Delta u^{cr}$ curve are straight lines. The depth, $h = 0.2$ m, the notch depth, $a = 0.05$ m and the beam span, $l = 0.8$ m were used as the geometry of the beam. The analysis is a plane stress analysis with the width of 1 unit. The initial boundary element mesh contains 73 nodes with 33 elements. The crack extension length is chosen to be 10 mm.

In Fig. 4 the fracture zone and the stress distribution in front of the crack tip are shown for different positions on the load–deflection curve. The fracture zone starts to develop as the specimen is subjected to the load. At the early stage of loading a small fracture zone has developed. The fracture zone further develops until the maximum load is reached, where the depth of the fracture zone is about 60 mm. The stress distribution at the maximum load is shown in Fig. 4(b).

It can be observed from this example that the material in front of the crack tip is still able to transfer stress even after the maximum load is reached. A traction free crack will not propagate until iteration 10 is reached, where the fictitious crack depth is about 100 mm. This indicates that for a material like concrete, there exists a noticeable fracture process zone in front of the real crack tip, which cannot be defined in material like metal. Therefore, the analysis of concrete using the fictitious crack model is reasonably accurate for analysing a crack propagation of standard beam sizes.

5.2 Example 2: comparison with FEM and experimental results

Among the variety of Mode I fracture experiments, the three–point bending of a notched beam, tested by Petersson [8], was selected for the analysis. The major advantage of this example is that this beam has been repeatedly used in experiments so that the necessary material parameters, such as fracture energy, G_F, are carefully specified. This allows the numerical results to be fairly matched with the experimental results. In the experimental investigation [8], six beams were tested in order to determine the value of G_F. The highest value of G_F obtained was 137 N/m and the lowest was 115 N/m. In the numerical analysis, the value of G_F of 124 N/m was chosen as a reasonable value to fit the experimental investigation. The beam is of depth $h = 0.2$ m, span length $l = 2.0$ m, thickness $b = 0.05$ m and the ratio between the notched depth and the beam depth, a/h, is chosen as 0.5. The material properties of the beam are $E_c = 30000$ MPa; $f_t' = 3.33$ MPa; $\nu = 0.2$ and $G_F = 124$ N/m. In the BEM analysis, the $\sigma - \Delta u^{cr}$ curve is assumed to be a linear straight line (SL) and a bilinear line (BL). The initial boundary element mesh is shown in Fig. 5(a) and contains 93 nodes with 41 elements. The analysis of the crack growth was performed by incrementing the crack length for 10 mm at every iteration. Figures 5(b) and (c) also shows the deformated shape of the beam for iteration 4 and 8.

The comparison of the numerical and experimental load–deflection curve is shown in Fig. 6 for the same value of G_F with two different shapes of the softening curve, namely a linear straight line (SL) and a bilinear line (BL). A good agreement was found for both BEM analysis and FEM analysis. An accurate match for the experiment is obtained when the bilinear line is applied. In contrast, the linear straight line leads to a solution that clearly falls outside the experimental scatter. Hence, for this type of concrete the bilinear line proposed by Petersson [8], obviously comes close to the experimental result and at least is a better presentation than the linear straight line. Therefore, it is shown that the numerical simulation for such types of fracture problems is found to be extremely sensitive to the input of the basic softening properties, i.e. the shape of the softening branch and the value of G_F.

5.3 Example 3: mixed mode problem – single notched

The first four examples were concerned with Mode I crack propagation employing a linear straight line (SL) and a bilinear line (BL). In this example, a more general case of mixed mode fracture in a single notched beam, tested by Arrea & Ingraffea [13], will be discussed. Fig. 7 shows the configuration of the beam. The condition of loading is non–symmetric, which implies that the fracture propagating from the notch will show opening as well as sliding (mixed–mode). In the experiments, the load was applied at point C of the steel beam AB and was controlled by a feedback mechanism, with the crack mouth sliding displacement (CMSD) as a control parameter. CMSD refers to the relative displacement measured along the vertical direction between notch surfaces. In the numerical analysis the control parameter was the crack length increment. In this example the crack length increment was taken as 20 mm. The concrete was modelled as linearly elastic in compression with the following parameters: $E_c = 24800$ MPa, $\nu = 0.18$, $f'_t = 2.8$ MPa and $G_F = 100$ N/m. The beam had a thickness of 0.156 m.

The BEM results was compared with the two FEM results, firstly by Rots & Blaauwendraad [14] who used a prescribed crack path and secondly by Alfaiate *et al.* [15] who used a non–prescribed crack path. For all analyses a bilinear line (BL) of softening curve was used. In BEM analysis the initial total number of nodes were 79 with 37 elements, as shown in Fig. 8(a). Also shown in Fig. 8 are the deformation shape for certain crack increments and finally the crack path, as shown in Fig. 9. From the deformation shape and the final crack path shown in Fig. 8 and 9, the BEM solution gives an excellent illustration of the real behaviour of a beam subjected to shear loading. As in the experimental investigation or in the FEM analysis, the crack path was predicted to propagate towards the load. This was also demonstrated in the BEM analysis.

The solution of the analysis is summarized in Fig. 10 and 11. Fig. 10 shows the load P against the crack mouth sliding displacement (CMSD). Fig. 11 shows the load P against the displacement at point C, which is the application of load. The displacement at point C is calculated from the displacement value at A and B using a suitable interpolation function by assuming that the steel beam

is infinitely stiff.

The results shown in Fig. 10 indicated that the pattern of the curves agreed for all of the analyses and it falls nicely within the experimental scatter at an early stage of loading, but started to deviate after the peak load was reached. The experimental results obtained by Arrea & Ingraffea [13] lie in the shaded area. In this figure, the load–CMSD curves obtained numerically by Rots & Blaauwendraad [14] and Alfaiate *et al.* [15] using FEM analysis were also shown. The former used a prescribed crack path while the latter used a non–prescribed crack path. In the analysis, Rots considered two approaches which were a discrete crack approach and a smeared crack approach. Using a smeared crack approach it was not possible to observe the post–peak region due to the numerical problems related with the model. The peak load obtained either by BEM or FEM analysis is smaller than the experimental. This may be due to the assumption that the aggregate interlock was not taken into account. When dealing with mixed mode problems, the presence of shear stress will also influence the results and somehow it must be taken as another cracking parameter.

In addition to the load–CMSD response, the load–deflection response has also been recorded, as shown in Fig. 11. The load–deflection curve exhibits a sharp snap–back behaviour. In the experimental investigation this snap–back can be detected if constant crack mouth sliding displacement is imposed. On the other hand, the snap–back behaviour can be captured numerically when using crack length increments as a controlling parameter. For a mixed mode problem, this scheme was applied by Carpinteri & Valente [8] in FEM analysis. The experimental load–deflection curves have not been reported by Arrea & Ingraffea [13], so that a direct comparison with the experimental results is not possible. However, the curve produced by the BEM analysis agreed well with the FEM analysis.

6 Conclusion

From this paper it can be concluded that the dual boundary element formulation in conjunction with fictitious crack model has been developed and shown computationally effective to analyse crack propagation in concrete. The use of the fictitious crack model to

represent the fracturing process in concrete seemed to agree well with the experimental results. However, the type of the softening properties demonstrated by the stress–deformation curves also played an important role. Two types of stress–deformation curves were tested which were a linear straight line (SL) and a bilinear line (BL). An accurate fit to the experiment is obtained when the bilinear line is applied.

References

[1] Brebbia, C.A., Telles, J.C.F. and Wrobel, L.C., *Boundary Element Techniques*, Springer–Verlag, Berlin and New York, 1984.

[2] Aliabadi, M.H. and Rooke, D.P., *Numerical Fracture Mechanics*, Comp. Mech. Publications and Kluwer Academic Publishers, 1991.

[3] Cruse, T.A., *Boundary Element Analysis in Computational Fracture Mechanics*, Kluwer Academic Publishers, Dordrecht, 1988.

[4] Portela, A., Aliabadi, M.H. and Rooke, D.P., The dual boundary element method: Effective implementation for crack problems, *Int. J. Num. Meth. Engng.*, **33(6)**, 1269–1287, 1992.

[5] Cen, Z. and Maier, G., Bifurcations and instabilities in fracture of cohesive–softening structures: a boundary element analysis, *Fatigue Fracture Engng. Mater. Structures*, **15**, 911–928, 1992.

[6] Saleh, A.L. and Aliabadi, M.H., Crack growth analysis in concrete using boundary element method, *Engng. Fracture Mechanics*, **51(4)**, 533–545, 1995.

[7] Hillerborg, A., Modeer, M. and Petersson, P.E., Analysis of crack formation and crack growth in concrete by mean of fracture mechanics and finite elements, *Cement and Concrete Research*, **6**, 773–782, 1976.

[8] Petersson, P.E., Crack growth and development of fracture zone in plain concrete and similar materials, *Report TVBM–1006*, Lund Institute of Technology, Lund, Sweden, 1981.

[9] Ingraffea, A.R. and Gerstle, W.H., Nonlinear fracture models for discrete crack propagation, in *Application of Fracture Mechanics to Cementitious Composites*, (ed. S.P. Shah), pp. 247–285, Martinus Nijhoff, Dordrecht, 1985.

[10] Carpinteri, A. and Valente, S., Numerical modelling of mixed mode cohesive crack propagation, *Int. Conf. on Computational Engng. Science*, (12–VI), Atlanta, GA, 1988.

[11] Gerstle, W.H. and Xie, M., FEM modelling of fictitious crack propagation in concrete, *J. Engng. Mech., ASCE*, **118(2)**, 416–434, 1992.

[12] Saleh, A.L., Boundary element formulation for crack growth analysis in concrete structures, PhD. thesis, Wessex Institute of Technology, Southampton, U.K. 1995.

[13] Arrea, M. & Ingraffea, A.R., Mixed–mode crack propagation in mortar and concrete, Report 81–13, Dept. Struct. Engng., Cornell Univ., Ithaca, New York, 1982.

[14] Rots, J.G. & Blaauwendraad, J., Crack models for concrete: discrete or smeared? Fixed, multi–directional or rotating?, *HERON*, **34(1)**, 1–59, 1989.

[15] Alfaiate, J., Pires, E.B. & Martins, J.A.C., Non–prescribed discrete crack evolution in concrete: algorithm and numerical tests, *Localized Damage III, Computer–Aided Assessment and Control*, eds. M.H. Aliabadi, A. Carpinteri, S. Kalisky & D.J. Cartwright, pp. 185–192, Comp. Mech. Pub., Southampton, U.K. 1994.

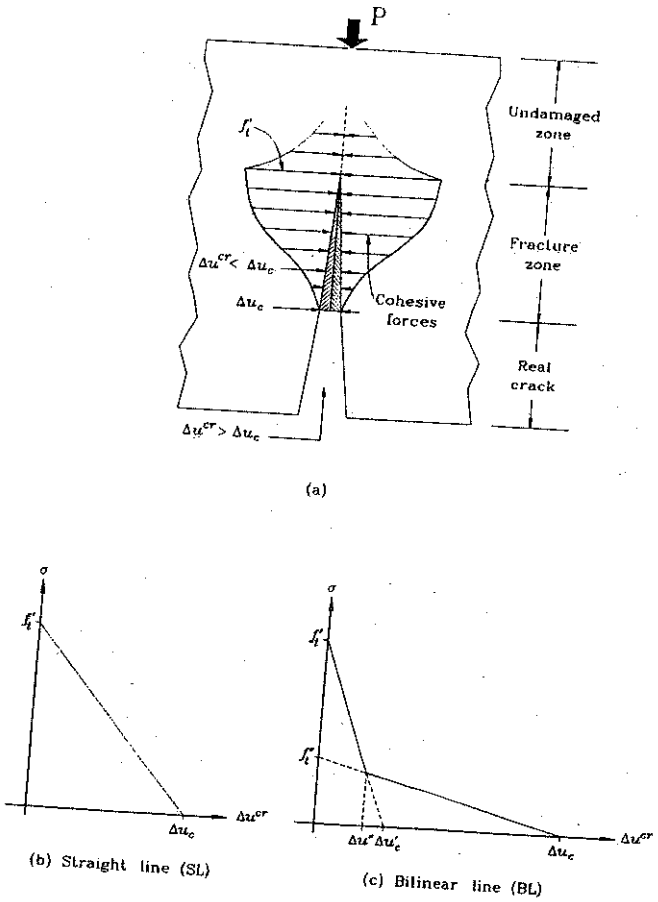

Figure 1: The fictitious crack model. (a) The fracture zone is replaced by the cohesive forces. The relationship of $\sigma - \Delta u^{cr}$ curve for (b) straight line (SL) and (c) bilinear line (BL).

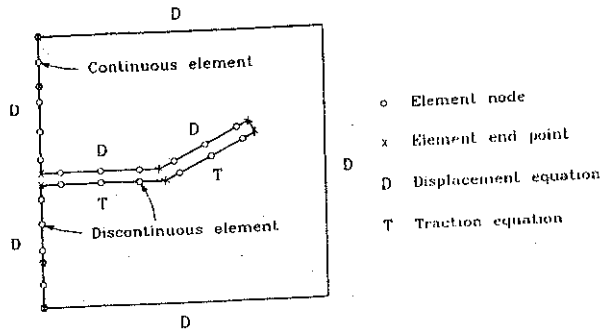

Figure 2: General modelling strategy of the dual boundary element method.

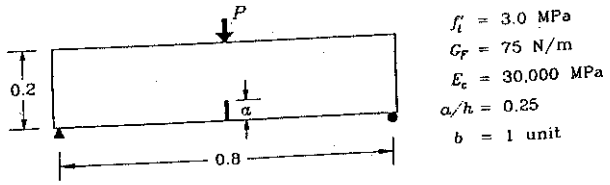

Figure 3: The notched beam subjected to the three-point bending and its material properties.

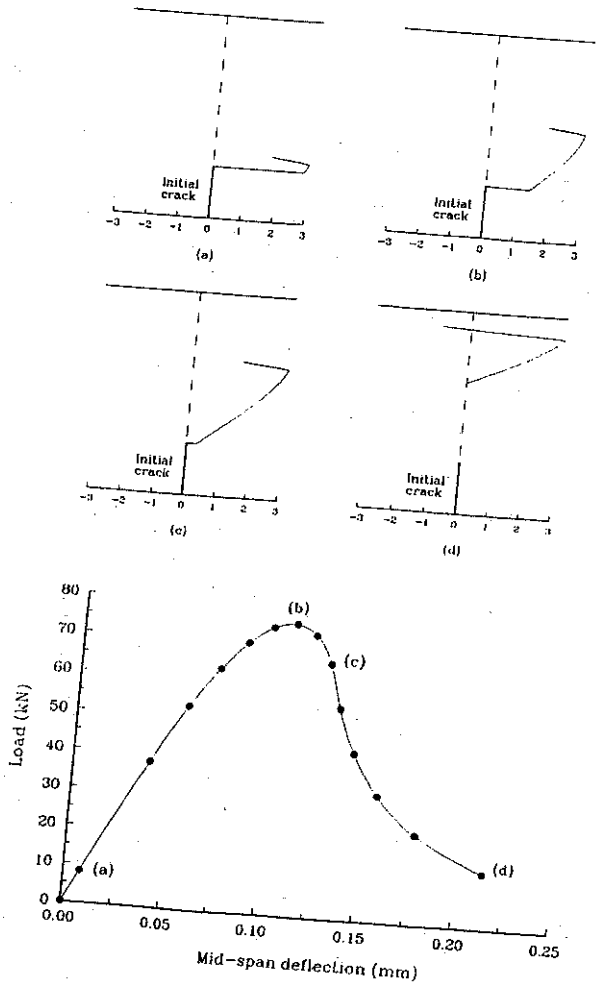

Figure 4: The fracture zone and stress distribution in front of the crack tip for different load levels of the load-deflection curve.

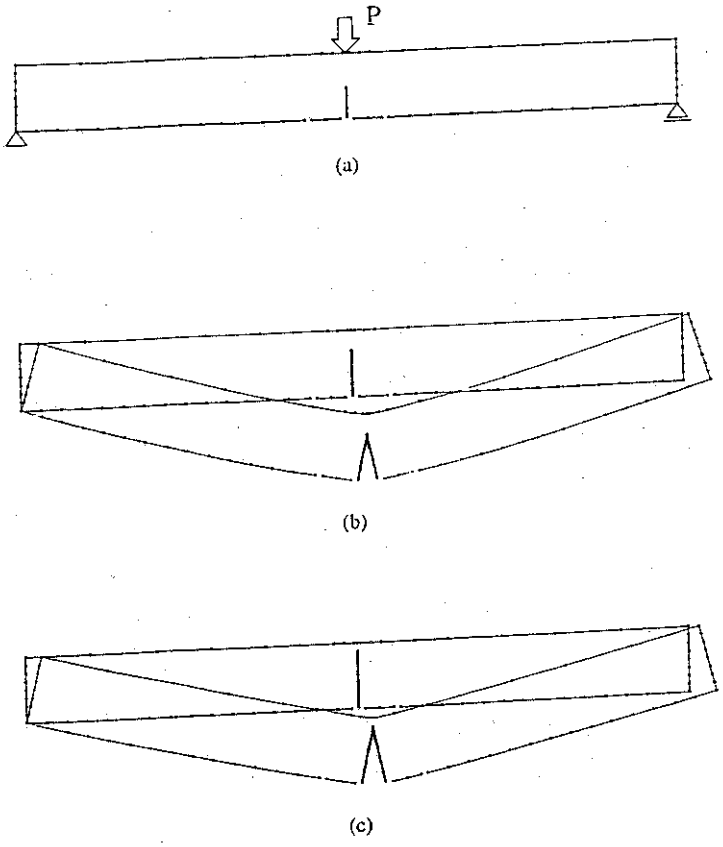

Figure 5: (a) Initial boundary element mesh and deformed shape for (b) iteration 4 and (c) iteration 8.

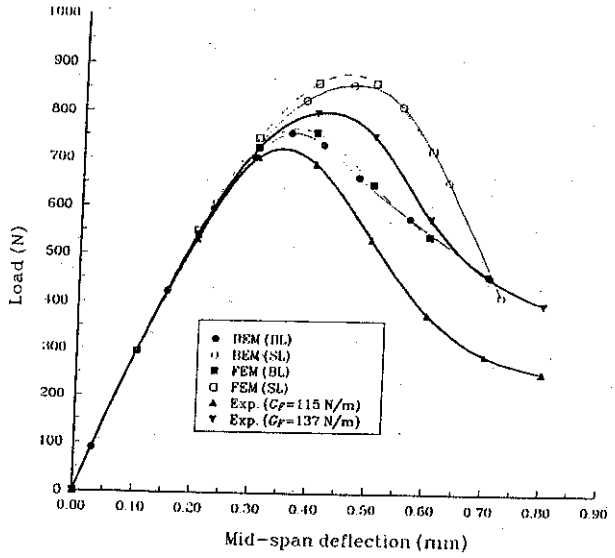

Figure 6: Load–deflection curve for three–point bending notched beam. Comparison with FEM and experimental results by Petersson [8].

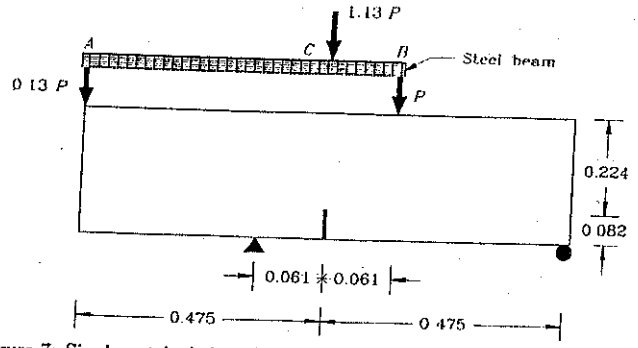

Figure 7: Single notched shear beam for mixed mode crack propagation.

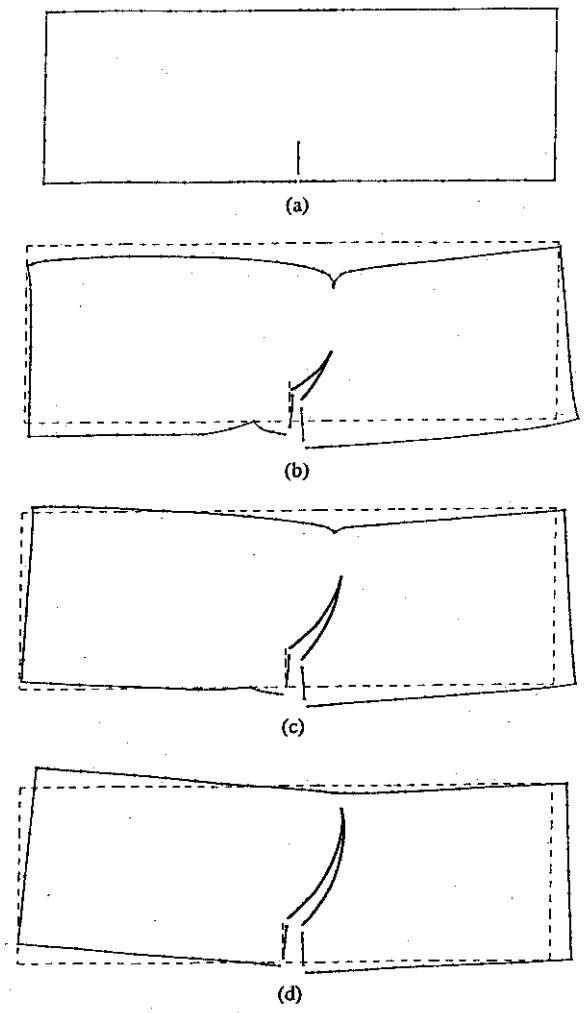

Figure 8: (a) The initial boundary element mesh and the deformation of the beam at (b) iteration 5, (c) iteration 8 and (d) iteration 11.

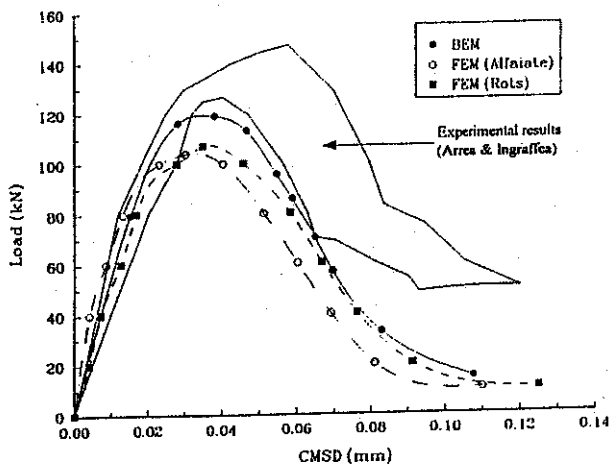

Figure 10: Load P against crack mouth sliding displacement (CMSD) of a single notched shear beam. Shaded area denotes range of experimental results.

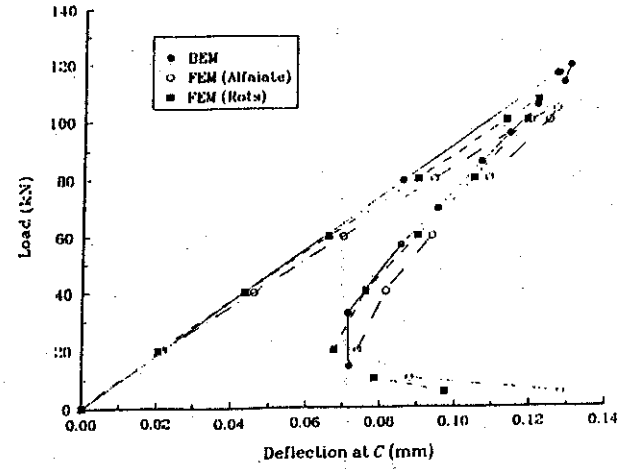

Figure 11: Load P against deflection at point C of a single notched shear beam.

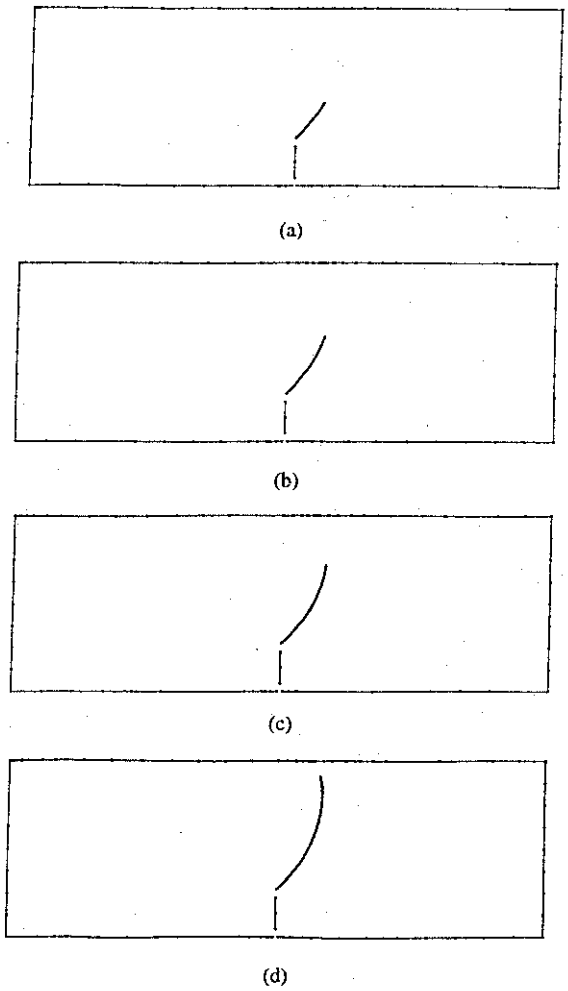

Figure 9: The crack path at (a) iteration 4, (b) iteration 6, (c) iteration 8 and (d) iteration 10.